

Designing a Drug to Inhibit Death-Associated Protein Kinase 1's Catalytic Activity

Paula Godoy

June 11, 2014

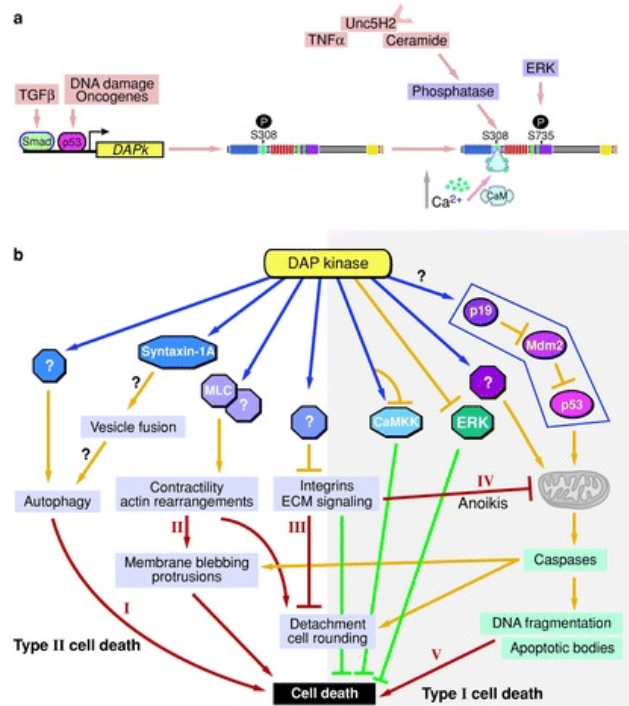
1 Introduction

Death-associated protein kinase 1 (DAPK1) is a Ser/Thr kinase regulated by the Ca²⁺/calmodulin cellular mechanisms. It coordinates several cell-death signalling pathways.

DAPK1 belongs to a family of Ser/Thr kinases all of which are regulated by CaM, a Ca²⁺-dependent pathway. All of these proteins contain high homology in their catalytic domain, especially with the related kinases ZIPK and DRP-1, of which DAPK1 shares around 80% amino acid identity in the catalytic region[1][2]. All of these kinases share a death-associated domain but differ in their extracellular regions important for localization and other differing activities[3]. The DAPK family is most closely related to other CaM-regulated kinases, such as myosin light chain kinase, which it shares 44% sequence homology in the catalytic region[1].

Because of its role in apoptosis, DAPK1 is recognized as a tumor suppressor gene. When it is not mutated, DAPK1 impedes tumorigenesis and subsequent metastasis. However, when DAPK1 is mutated, it can allow for unregulated cell growth without consideration towards apoptotic pathways. Its loss of expression has been found in multiple tumor types. Studies have shown that DNA methylation is the culprit behind inhibiting DAPK1 expression, and this has provided a target for cancer therapies. Drugs like Decitabine can reverse DNA methylation and allowing for continued expression of previously-silenced genes. Although these drugs are approved, they are highly unstable and are not orally available[2].

DAPK1 is also found in large quantities in the central nervous system and has been associated with diseases caused by neuronal injury; because of this association, it may be targeted to prevent neurodegeneration, a symptom of many cognitive debilitating diseases[1]. Because of its role in neuronal death, DAPK1 has been suggested as a possible target to reverse the large scale death of neurons following stress to the brain or through other genetic causes[2]. There have been two approaches to target DAPK1 for therapeutic reasons, involving neurodegeneration. The first approach targeted the inhibitory tail of DAPK1 (discussed in the Structure section of this paper). They synthesized a similar peptide and covalently linked it to tetramethylrhodamine isothiocyanate, increasing the peptide's hydrophobicity so that it may be absorbed by cells. This mechanism allowed for the protection of hippocampal neurons when induced by cell-death pathways[2].



Bialik S, Kimchi A. 2006. Annu. Rev. Biochem. 75:189–210

Figure 1: This image shows the several signalling pathways associated with DAPK1 and how they are all coordinated towards cell-death[1]. Image taken from Reference 1.

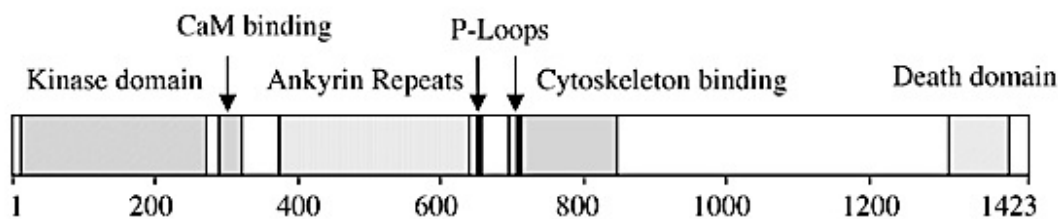


Figure 2: One-dimensional schematic of DAPK1 corresponding to the primary sequence and location of the several domains and motifs[2].

The second approach used rational design to create small chemical compound inhibitors that impeded the catalytic activity of DAPK1. They reported an IC_{50} of 13 μ L with their alkylated 3-amino-6-phenylpyridazine. This inhibitor shows some selectivity because its IC_{50} was 10-fold lower than other kinases, such as PKA or PKC. They proceeded to crystallize the inhibitor with DAPK1 and found that the drug partially engaged the ATP binding site[2].

2 Background

DAPK1 has the same general structure as seen in other kinases. It has two lobes: an N-terminal lobe with beta-sheets and a C-terminal lobe constructed mostly of alpha-helices. The ATP binding domain is constructed of beta-sheets and is between the N- and C-lobes. Lysine 42 is the amino acid required for binding onto ATP.

The catalytic domain contains clusters of acidic and basic residues. The acidic residues are located where the substrate binds, and the basic residues are seen at the phosphorylation site. This suggests an interaction between these different types of amino acids in substrate recognition[1]. The catalytic domain contains several conserved amino acids: Lys42, Glu64, Glu100, Glu143, Asn144, and Asp161. The carbonyl oxygen of Glu64 is hydrogen-bonded to the amino group of ATP. There are also four water molecules and only one metal ion that were found to be essential for catalysis[3].

DAPK1's kinase domain is followed by a CaM binding segment that can act competitively as a pseudosubstrate and inhibit catalysis. When CaM binds to Ca^{2+} , it binds to the CaM binding domain causing the autoregulatory segment is pulled out of the active site. Ser308 is subsequently phosphorylated, increasing affinity for calmodulin. This allows for DAPK1 to be highly active even when CaM levels are low[2][3]. DAPK1's (along with most other kinases) characteristic feature indicative activity or inactivity is the DFG motif. When phenylalanine is in the ATP-binding pocket, the kinase is on. When aspartate is in the ATP-binding pocket, the kinase is off. Figure 3 shows the ATP-binding pocket of a DAPK1 bound to calmodulin. Remember that calmodulin initiates a structural rearrangement causing DAPK1 to become active[1].

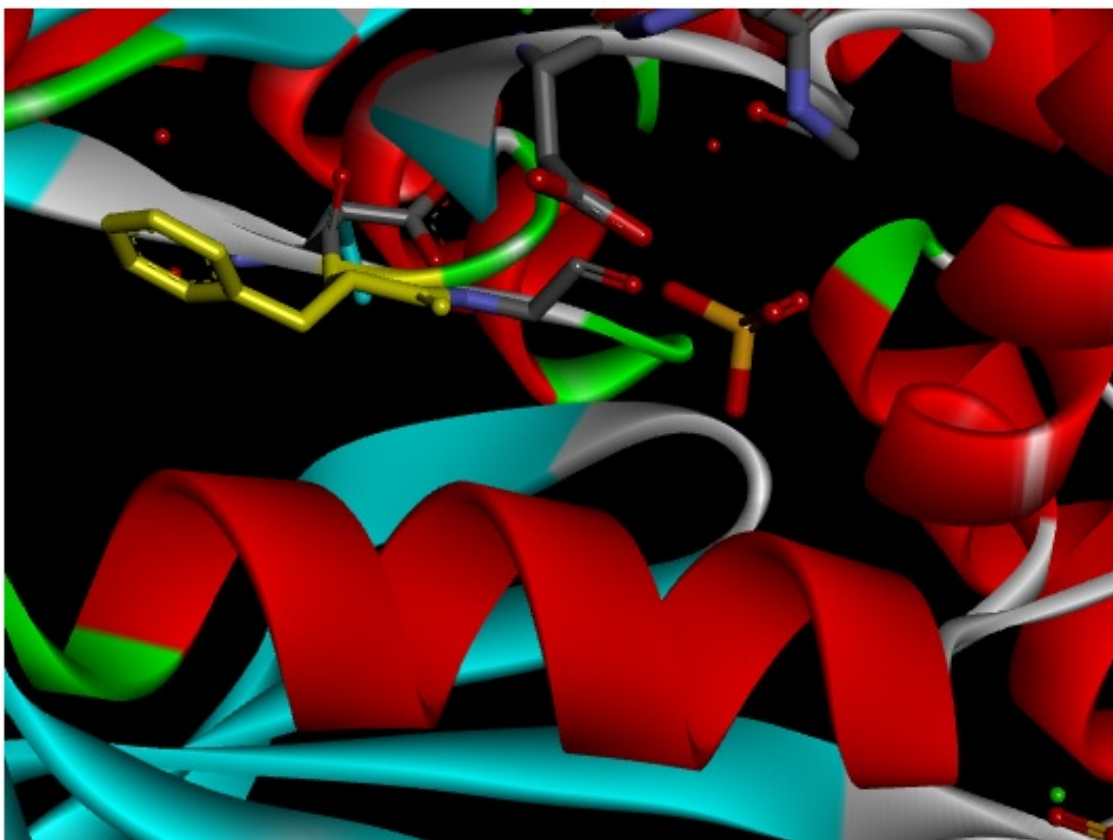


Figure 3: This image shows the structure of DAPK1 bound to calmodulin. Specifically, the image shows the ATP-binding site. The DFG motif are outlined as sticks and phenylalanine is highlighted in yellow to point out its location. Above the red α -helix is where ATP usually binds and is a target for many inhibitors (see next two figures). When phenylalanine is placed inside this region, it is ready to bind to ATP, indicating an active conformation. Binding of calmodulin causes a structural rearrangement rendering the kinase active. Generated through Accelrys Discovery Studio (ADS).

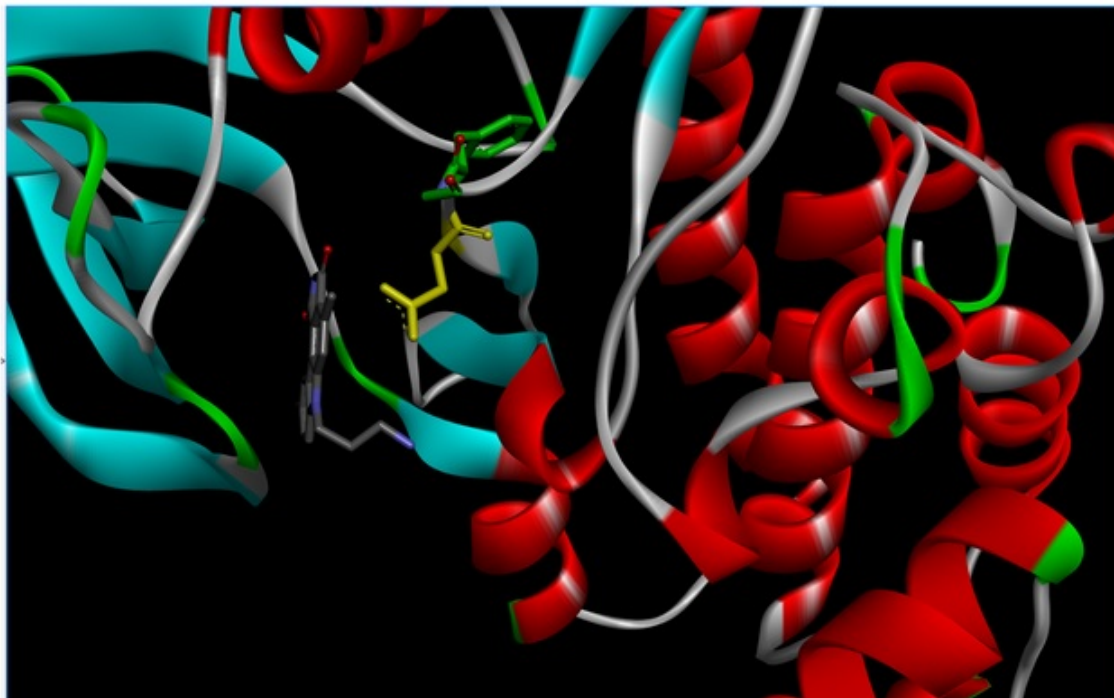


Figure 4: This image shows the structure of DAPK1 cocrystallized with a small inhibitor placed at the ATP-binding site. THE DFG motif is outlined as sticks and the aspartate is highlighted in yellow to emphasize the DFG-out conformation. Generated from ADS.

Figure 4 is an image of the DFG motif interacting with a small inhibitor. This structure is the structure seen in Figure 7. It is the structure that all pharmacophore and de novo ligands were generated from. In Figure 4, the aspartate is facing out, indicating a DFG-out conformation. This means the kinase is inactive.

Figure 5 shows the image of a known inhibitor of DAPK1 that contains high selectivity for DAPK1[4]. This inhibitor is called ruthenium octasporine ligand or OSV. OSV is located at the ATP-binding site and keeps the kinase in the DFG-out, or inactive, conformation. The ligand interacts with the aspartate residue.

Other domains include an eight ankyrin repeat. Ankyrins are proteins that coordinate the attachment between actin and membrane-bound proteins. This suggests that DAPK1 is an action-associating protein because it can bind to the cytoskeleton[1][2]. The eight ankyrin repeat is made up of 33 amino acid repeats. The ankyrin repeats extend from residues 378-641.

From DAPK1's N-lobe, a loop extends composed of highly ordered, positively charged basic residues. 12 of these residues are a highly conserved characteristic seen throughout the DAPK family. The upper lobe is not required for binding to the substrate[1][2]. DAPK1 also contains two P loops that do not have a classified function but are believed to interact with other peptides[2][3].

The C-terminal domain is composed of a death domain succeeded by a 17 amino acid long tail rich in Serines. This Serine-rich tail is commonly seen in proteins with a death domain. The death domain has a regulatory purpose that negatively regulates DAPK1 function. The

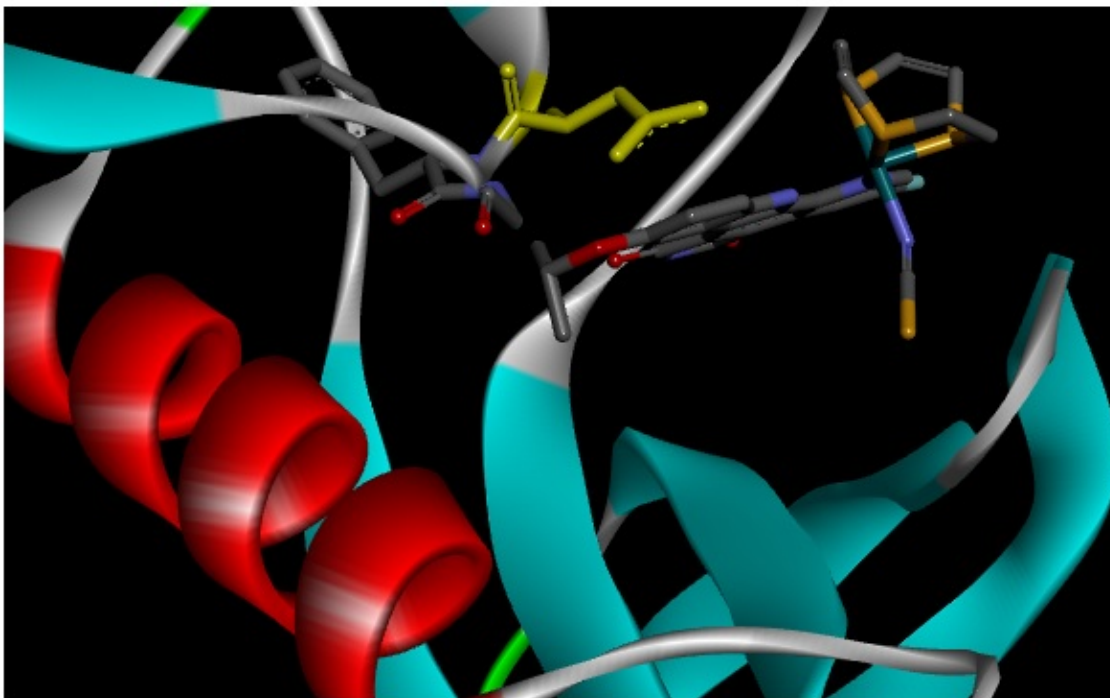


Figure 5: This image shows the structure of DAPK1 cocrystallized with OSV. OSV is placed at the ATP-binding site and keeps the DFG motif in its outward conformation. This keeps the kinase inactive.

death domain consists of residues 1311-1396.

The glycine-rich region (LGSGQFAVV) is located at the N-terminus of the protein. The hinge region are two other conserved motifs seen in kinases. The glycine-rich region is essential for catalytic activity. It's required for structural movements that allow for optimal substrate binding and increased selectivity of kinases[4]. When mutated, a decrease in activity is observed [5]. The hinge region connects the N-lobe and C-lobe and is spatially proximal to the glycine-rich region. It has been targeted by small metals to simulate ATP binding while also showing high selectivity to the hinge region of DAPK1[5].

3 Approach

The structure used to design the DAPK1 inhibitor was a crystal structure of the kinase domain bound to a small molecule inhibitor (PDB ID: 1WVX)[6]. This structure did not have any accompanying paper describing the structure but was only one of few structures that contained an inhibitor. The idea behind creating our drug was to capture the structure in an inhibitory position and create a small compound molecule that fit in a similar fashion as the known inhibitor.

Figure 8 shows the receptor-ligand interactions between the small inhibitor and receptor seen in Figure 7. The intermolecule interactions are composed mostly of pi-alkyl bonds between polar atoms and the aromatic rings (purple dashed lines). The green-dashed lines represent hydrogen bonds between non-water molecules.

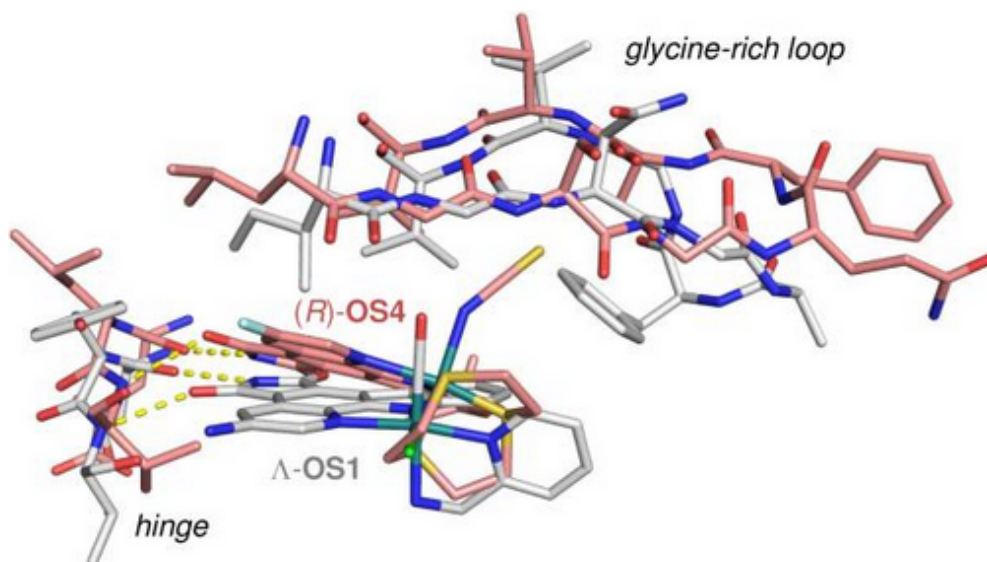


Figure 6: This image was taken from the article in Reference 4. It shows the glycine-rich loop interacting with OSV, the inhibitor ligand discussed in Figure 5, and the hinge region of DAPK1. This interaction inhibits kinase activity.[4]

Figure 9 shows the hydrophobicity levels at the site of the receptor-ligand interactions. The binding pocket is more hydrophobic than the outer edges of the pocket. We expect the outer edges of the binding pocket to be more soluble than the internal section of the receptor. The aromatic rings may also contribute to this hydrophobicity.

Two different approaches were used to generate a ligand library via Accelrys Discovery Studio: using pharmacophores and using *de novo* fragment generation.

For the pharmacophore-based approach, a pharmacophore was generated automatically using the receptor-ligand interactions between the known inhibitor seen in Figure 7 and the rest of the kinase domain of DAPK1. Once the pharmacophore was generated, it was screened using the chemdiv library. This outputted several different ligands in several different conformations. All of these were docked onto the receptor using Libdock. The top five ligands were chosen based on their Libdock score. These five ligands were then inputs for the second ligand docking procedure using a more optimized docking algorithm, CDOCKER. CDOCKER also outputted these five ligands in many different conformations. The top scoring CDOCKER energy ligand was used as the final ligand. Figure 8 shows the pharmacophore and the final ligand generated from this procedure.

For the *de novo* ligand-based approach, the *de novo* receptor protocol was used. This generated only one ligand named GU3. This was used as the ligand for the *de novo* link protocol. Thirteen ligands were outputted once this procedure finished running. These ligands were all fragmented, so bonds were created and destroyed in order to create a rationally designed ligand without weird bond angles. The ligands were then inputted into a energy minimization protocol. These edited ligands were then docked using Libdock; the top five highest scoring ligands were then run on CDOCKER and the final *de novo* based ligand was

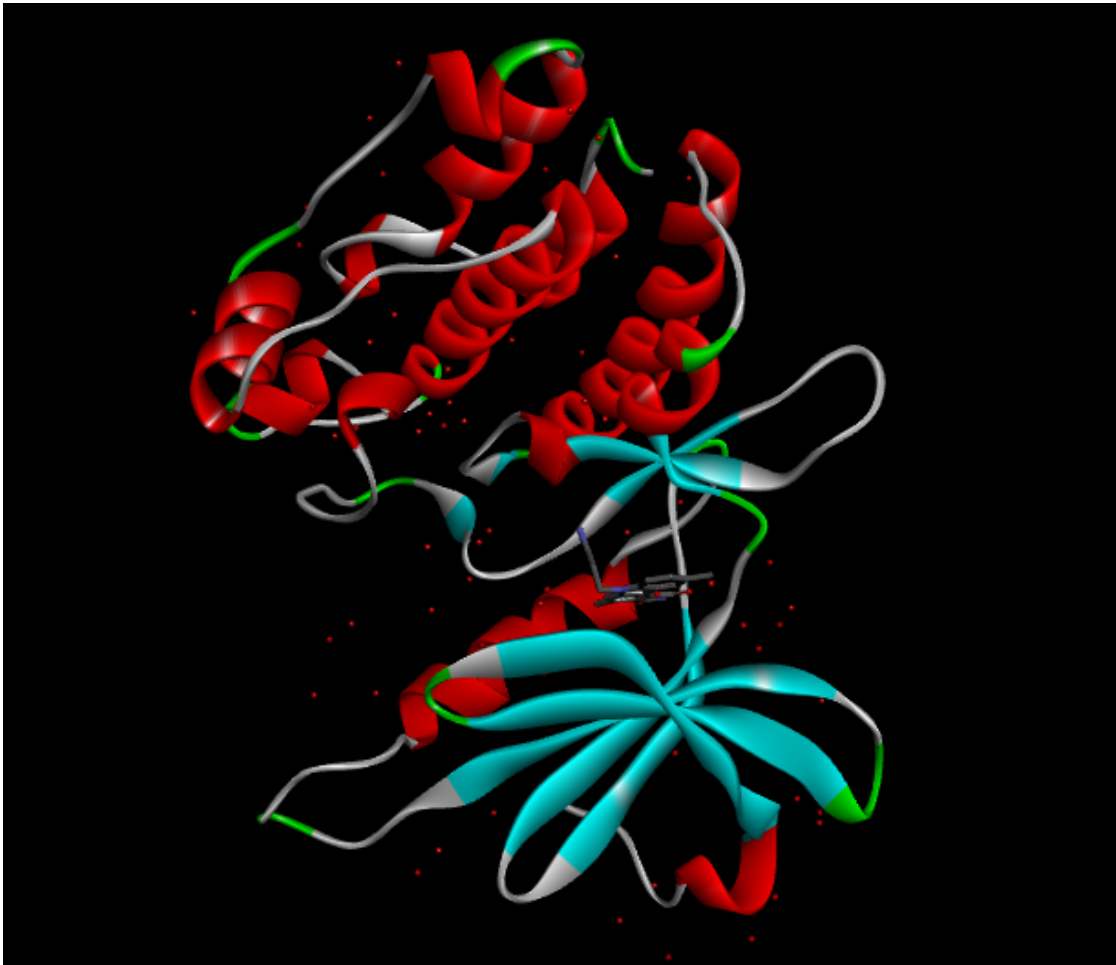


Figure 7: This structure was obtained from PDB[6]. It portrays the kinase domain of DAPK1 bound to a small molecule inhibitor. This inhibitor binds in the ATP-binding site and keeps the kinase inactive. Image generated with Discovery Studio.

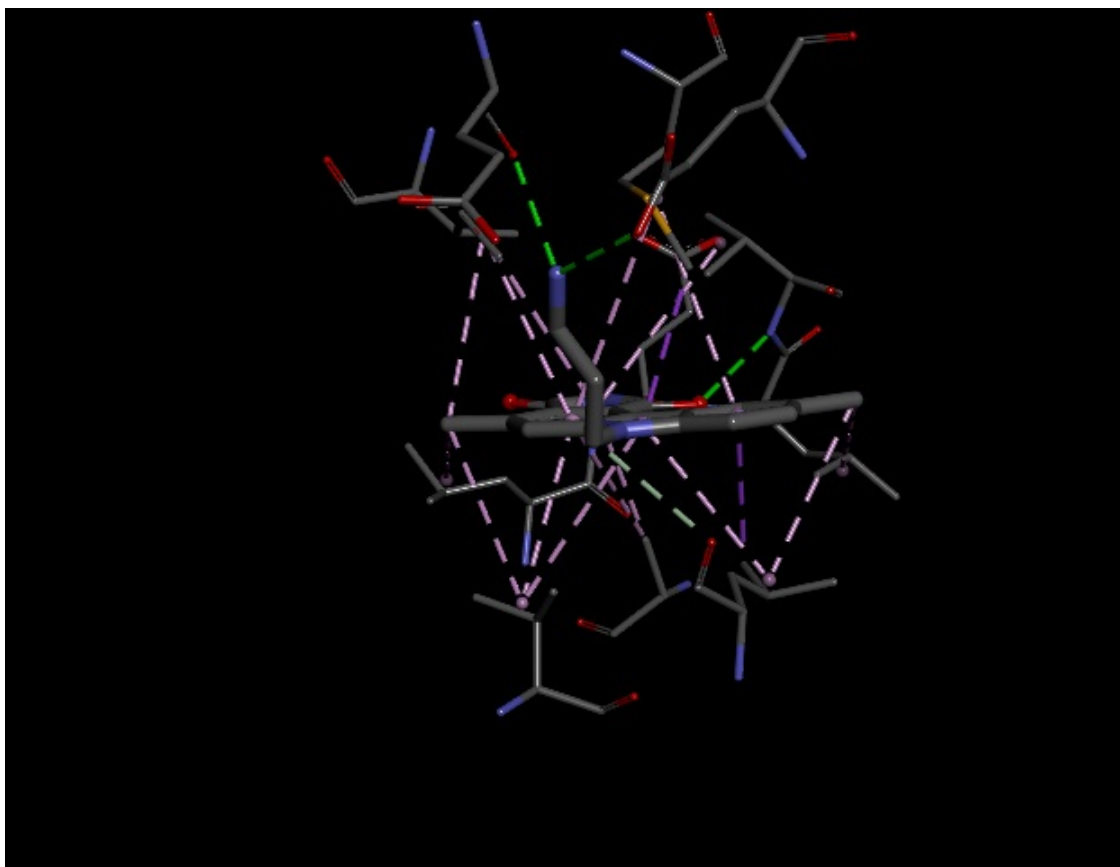


Figure 8: This image shows the receptor-ligand interaction between the small-molecule inhibitor seen in the figure above and the receptor. The green dashed lines represent hydrogen bonds between non-water molecules while the purple dashed lines represent pi-alkyl bonds. The ligand is in the center of the image with the receptor residues portrayed as lines around the ligand.

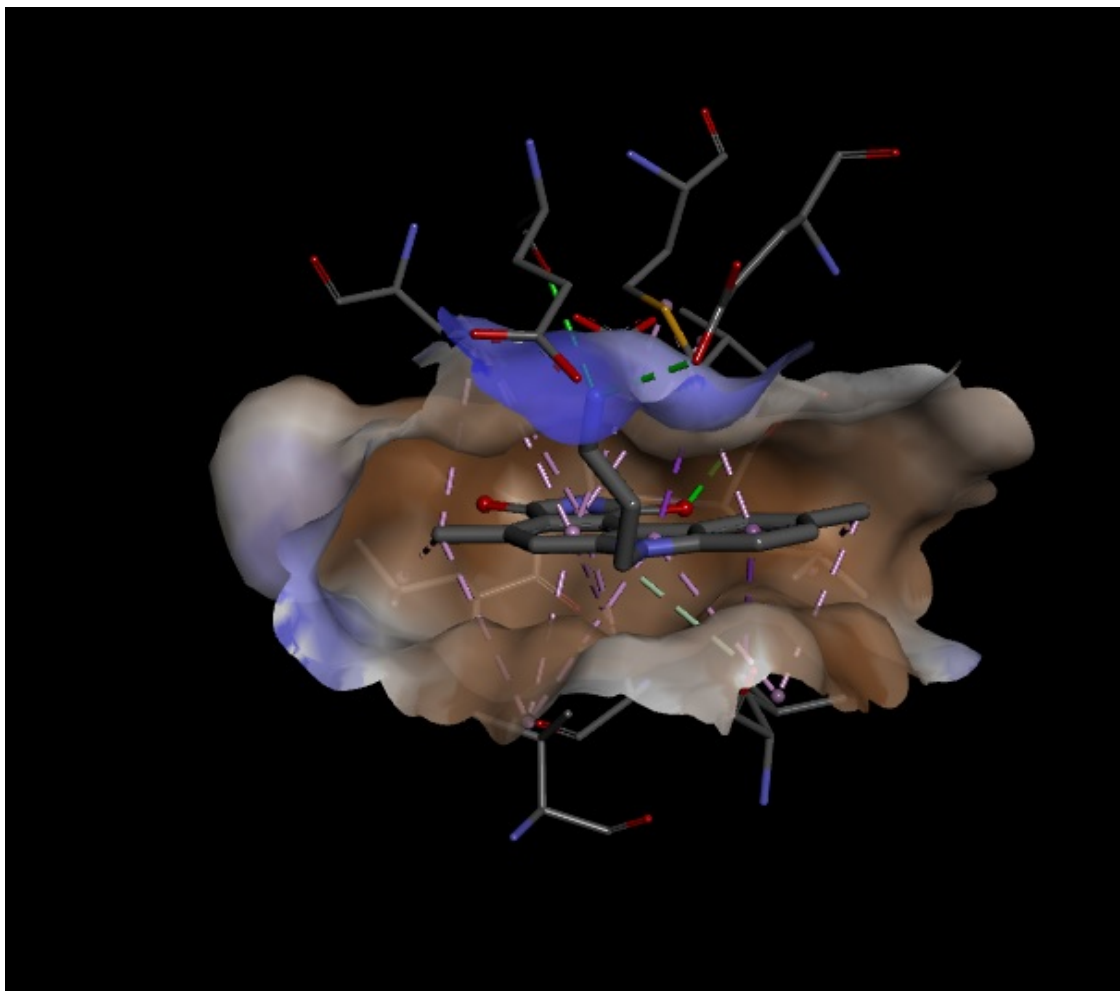


Figure 9: This image shows the receptor-ligand interaction between the small-molecule inhibitor seen in the figure above and the receptor. This highlights the hydrophobic areas of the interaction. The binding pocket is hydrophobic while the outer edges of the pocket are more neutral in hydrophobicity. Shades of brown indicate regions of high hydrophobicity, with white being areas of neutral, and blue being areas of low hydrophobicity.

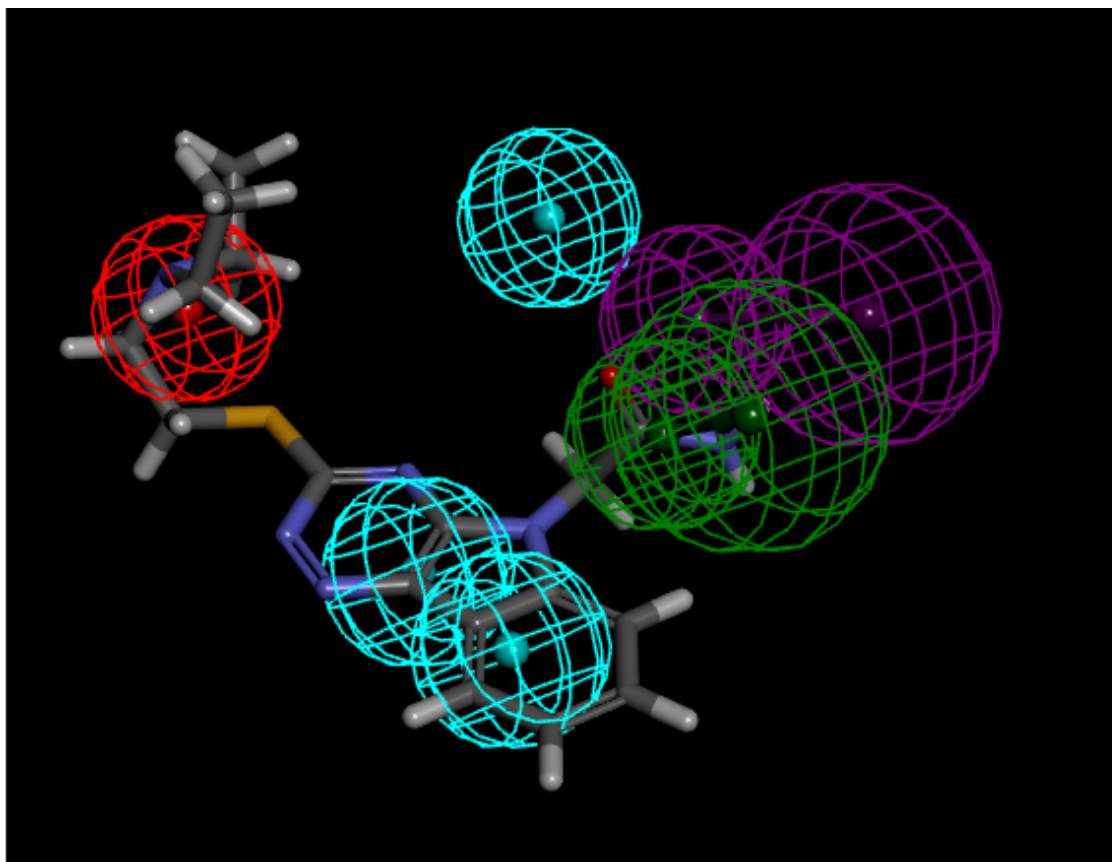


Figure 10: This image shows the pharmacophore generated automatically using a receptor-ligand interaction of DAPK1 bound to a small molecule inhibitor. The final ligand with the best Libdock and CDOCKER score is also present in this figure. The light blue cage represents hydrophobic regions. The green cages represents hydrogen bond acceptors; the purple cages represent hydrogen bond donors. The red cage represents positively charged ionizable functional groups. In this case, it is an amine group.

chosen. These structures are analyzed in the following section.

4 Results

4.1 The Pharmacophore Ligand

Figure 10 shows an image of the pharmacophore for the optimal ligand chosen during this procedure. The pharmacophore is made mostly of hydrophobic regions and hydrogen bond donors and acceptors. There is only one positively charged ionizable group. This makes sense as the binding pocket consists mostly of hydrophobic regions.

Figure 11 shows the pharmacophore ligand generated after two ligand docking algorithms. This ligand has a different conformation than the ligand seen in Figure 10 but is the same molecule. It is a relatively large molecule compared to the small-molecule inhibitor seen earlier in Figures 7-9.

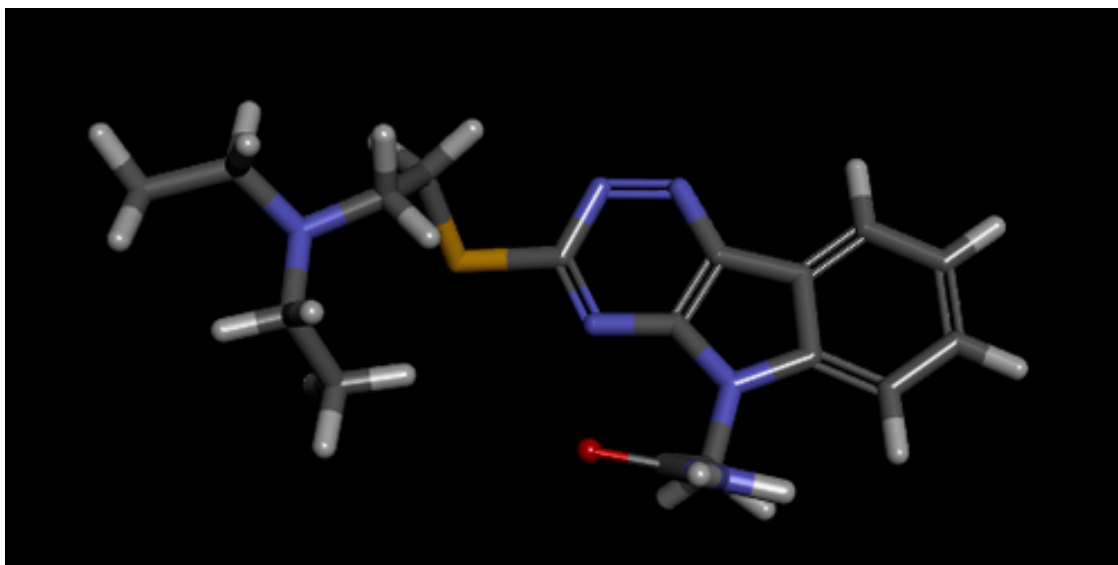


Figure 11: Pharmacophore ligand only. The yellow atom represents a sulfur atom; blue is for nitrogen; and red is for oxygen. This ligand is structurally similar to an ATP analogue except the charge is distributed throughout the molecule rather than solely at the triphosphate region.

Figure 12 shows receptor-ligand interactions between the pharmacophore and DAPK1. This ligand incorporates many more intermolecular interactions than the small-molecule inhibitor seen in Figure 8. This may suggest that the binding potency will be stronger, and thus the inhibitor effect of the ligand will be more powerful. It also contains two different kinds of pi-interactions rather than just pi-alkyl bonds.

Figure 13 shows the hydrophobicity levels at the site of the receptor-ligand interaction. As seen previously in Figure 9, the binding pocket is more hydrophobic than the outer edges of the pocket, since it is not exposed to the outside environment. This binding pocket looks slightly more hydrophobic than Figure 9. This may be due to added hydrophobic features of the pharmacophore ligand, especially since it doesn't have the highly charged triphosphate tail. Instead it contains three aromatic rings and a tail composed mostly of carbon atoms with few polar atoms, like oxygen which is towards the outside of the pocket and like the amine group adjacent to the carbonyl oxygen. It seems like the software situated the ligand so that its most polar regions are facing away from the hydrophobic pocket.

Lastly, the free energies of the ligand, the receptor, and the receptor-ligand complex were calculated to determine the binding energy. The binding energy for the pharmacophore-generated ligand is -78.9 kcal/mol.

4.2 The *De Novo*-based Ligand

Figure 15 shows an image of the *de novo*-generated ligand. It is a lot smaller than the pharmacophore-generated ligand but is still highly composed of carbons and a few Nitrogens. This ligand contains only two aromatic rings but are highly hydrophobic.

Figure 16 shows the receptor-ligand interactions between DAPK1 and the *de novo*-

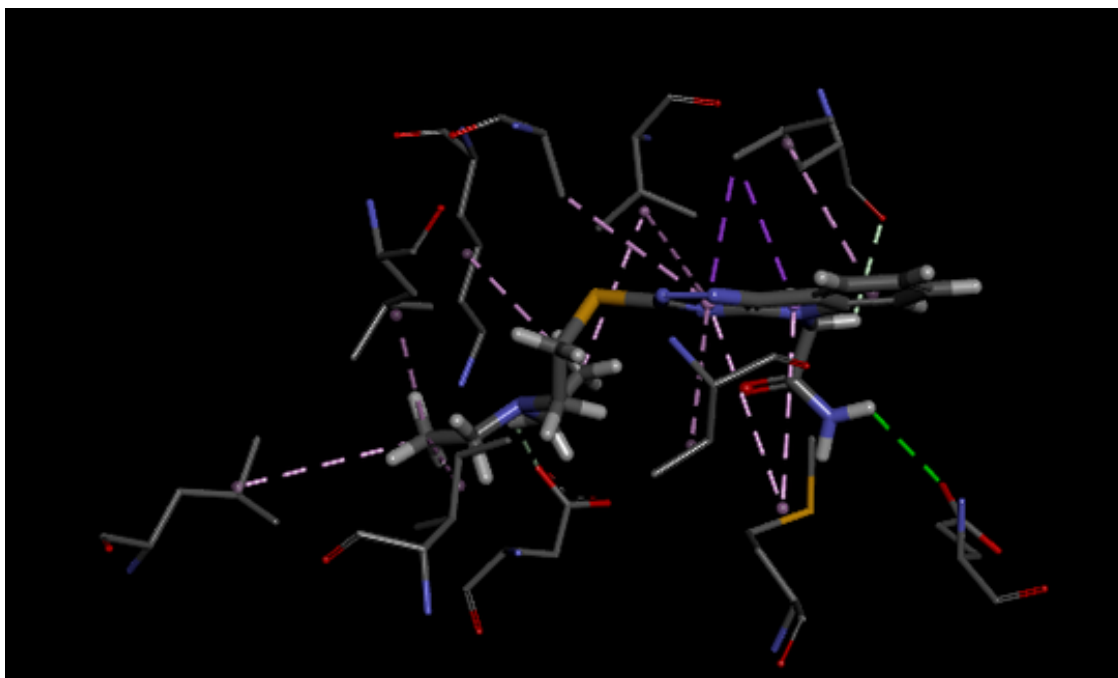


Figure 12: Receptor-Ligand Interactions with DAPK1 and the pharmacophore ligand. The light and dark purple dashed lines represents pi-interactions. Green dashed lines represents hydrogen bonds between non-water molecules.

generated ligand. As seen in the pharmacophore-generated ligand (Figure 12) and the small-molecule inhibitor (Figure 8), the majority of intermolecular interactions are pi-interactions. Less of the residues in the binding pocket are interacting with the ligand as compared to the pharmacophore-generated ligands which made contacts with many more residues. This may be a positive note in that there is a smaller probability of steric clash and a higher probability of permeability through cells. However, it may also decrease the probability that the ligand will remain in the binding pocket for a longer amount of time, as compared to the pharmacophore-generated ligand.

Figure 17 shows the hydrophobicity regions of the receptor-ligand interactions. The hydrophobic regions remained consistent through Figure 9 and Figure 13. The binding pocket is more hydrophobic than the outer edge, as expected.

Figure 18 shows the ADMET plot for the *de novo*-generated ligand. As explained above, the blue dot is in the center of the light blue circle, allowing for this information to be taken reliably (although this data is generated through predictive algorithms and must be taken as speculation). The *de novo*-generated ligand is centered in most of the circles, suggesting that it is orally bioavailable.

Lastly, the free energies of the ligand, the receptor, and the receptor-ligand complex were calculated to determine the binding energy. The binding energy for the *de novo*-generated ligand is -7 kcal/mol.

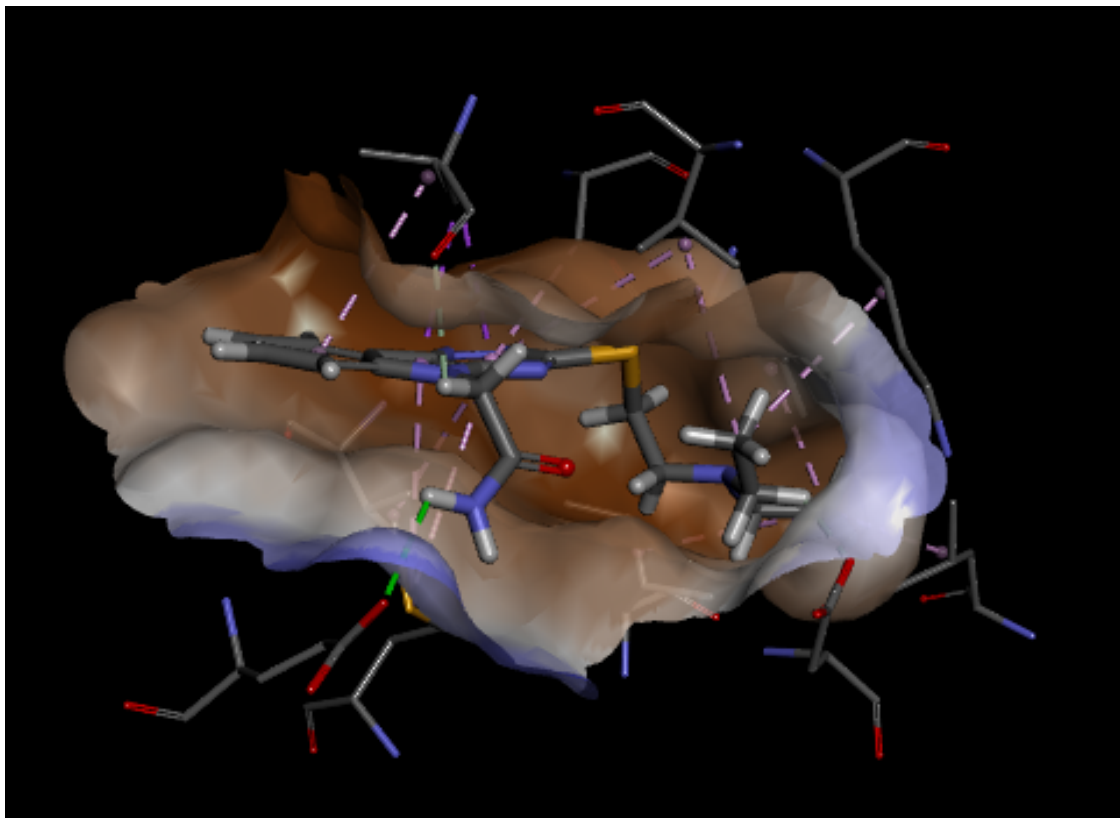


Figure 13: Hydrophobicity levels of the receptor-ligand interactions between DAPK1 and the pharmacophore-generated ligand. Areas of high hydrophobicity are depicted in shades of brown, with white being areas of neutral hydrophobicity, and shades of blue being areas of low hydrophobicity.

Discovery Studio allows for the calculation of molecular properties, in terms of its ADMET properties. ADMET stands for "absorption, distribution, metabolism, and excretion" [7].

The "T" in this case stands for toxicity. In Figure 14, the ADMET plot shows that the pharmacophore-generated ligand fits in the range of absorption and blood brain barrier permeability, as compared to other FDA drugs. A general standard is that if the blue dot is outside of the light blue circle, this prediction would be unreliable. However, in the case of this ADMET plot and the rest of the ones in this paper, the blue dot is seen inside the light blue circle. This suggests that the drug is orally bioavailable.

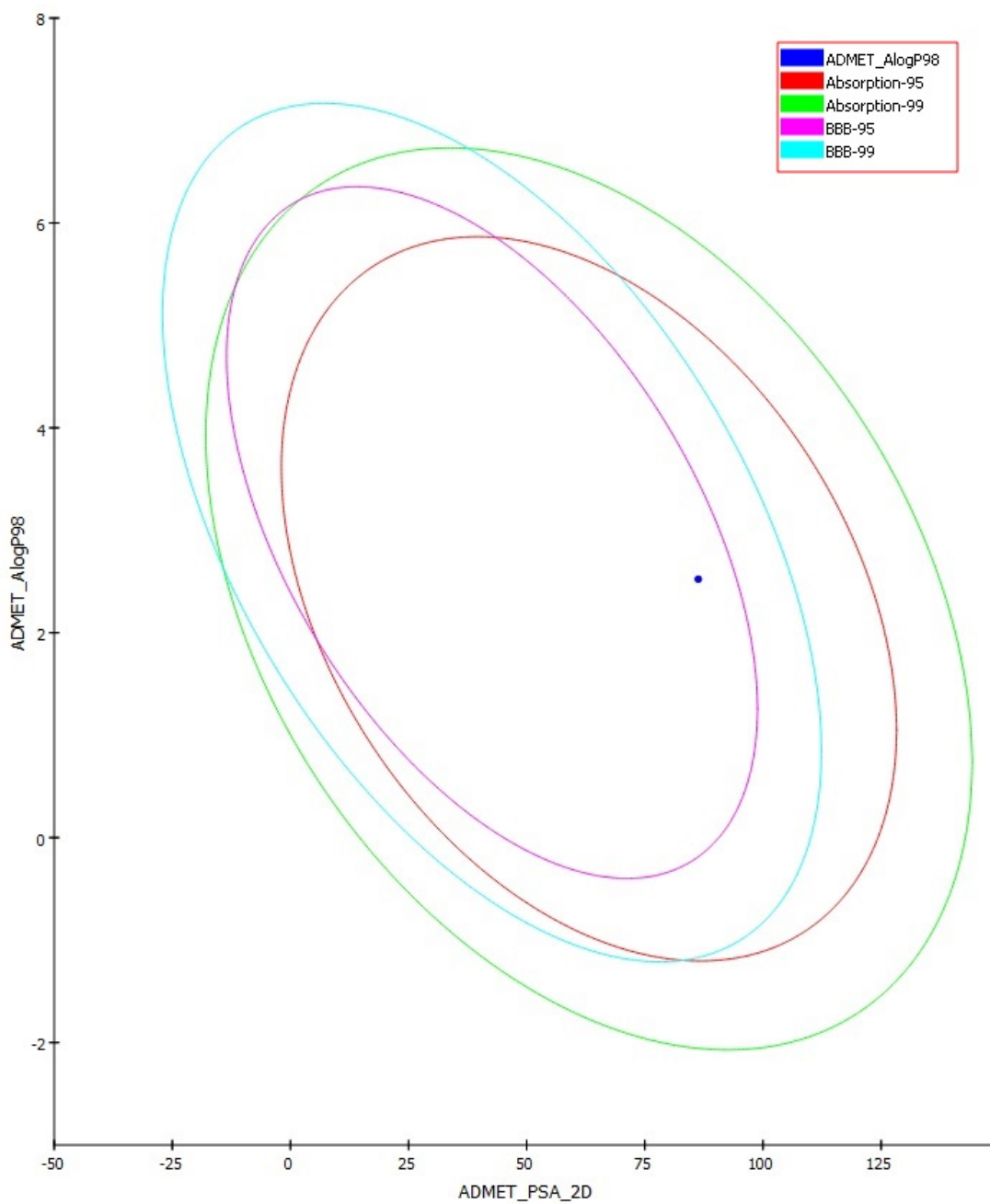


Figure 14: ADMET plot for the pharmacophore-generated ligand. The key at the top right indicates what each color refers to. The blue dot is the ADMET score of the pharmacophore-generated ligand as compared to the molecular properties calculated. The red and green circles refer to its absorption abilities. The purple and light blue circles refer to the permeability through the blood brain barrier.

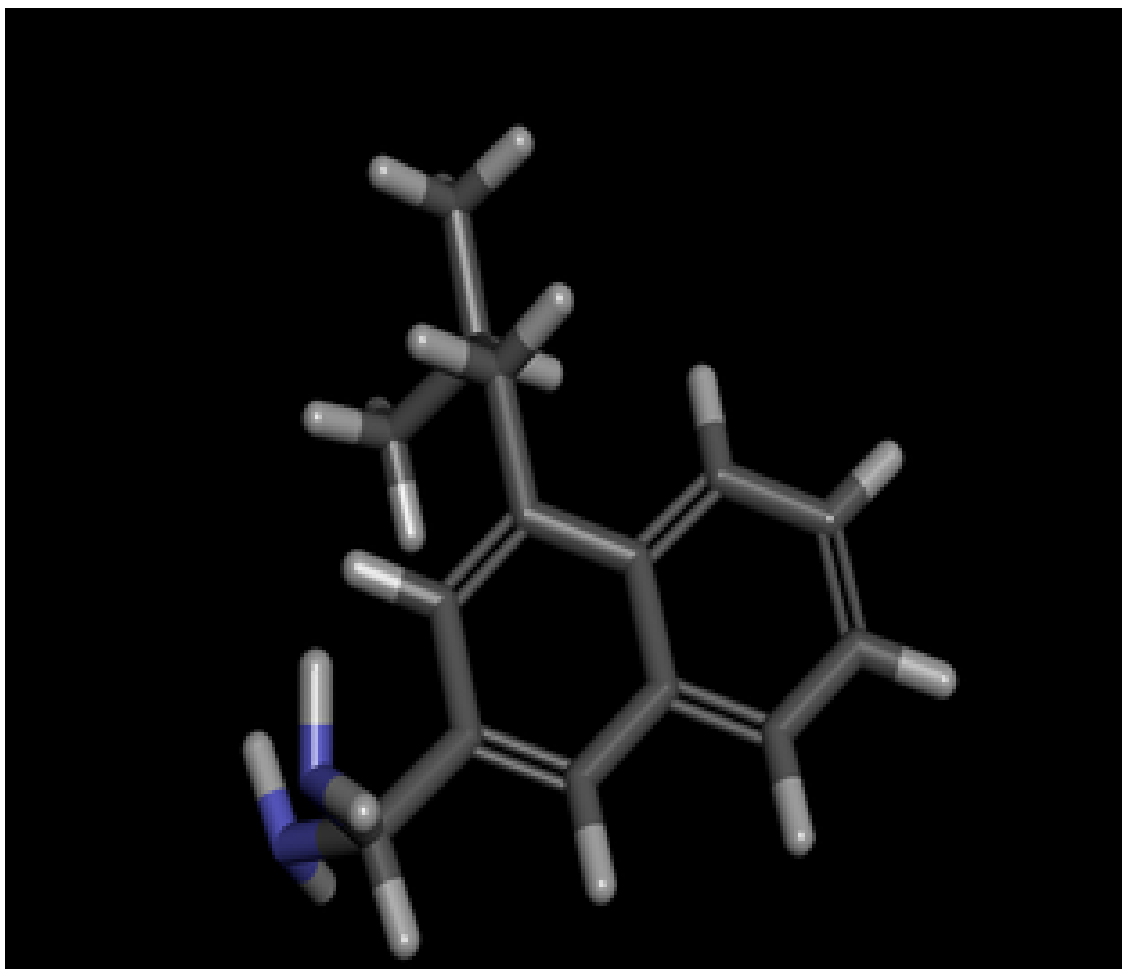


Figure 15: Image of *de novo*-generated ligands. Blue atoms represents Nitrogen; grey is carbon, and light grey is hydrogen.

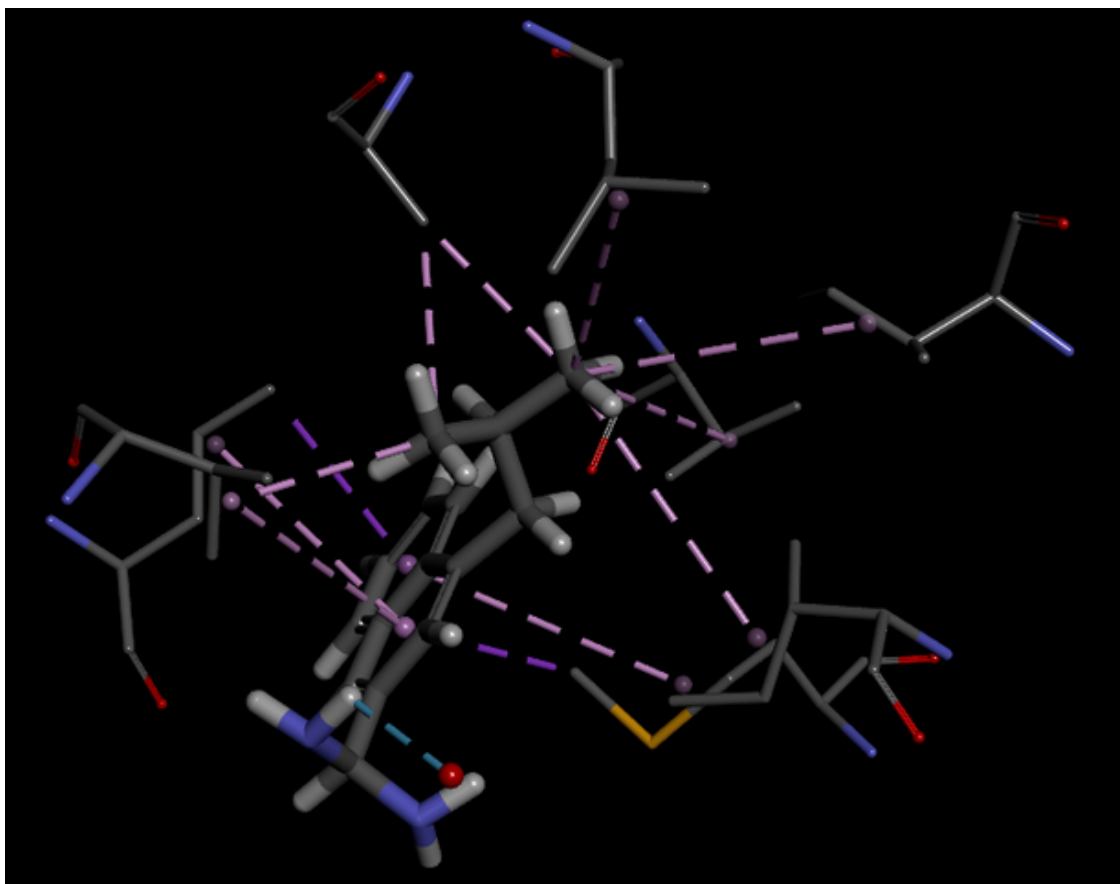


Figure 16: Receptor-ligand interactions between the *de novo*-generated ligand and DAPK1. Purple dashed lines represent pi-interactions. The ligand is in the center of the figure, with the residues of DAPK1 represented as lines.

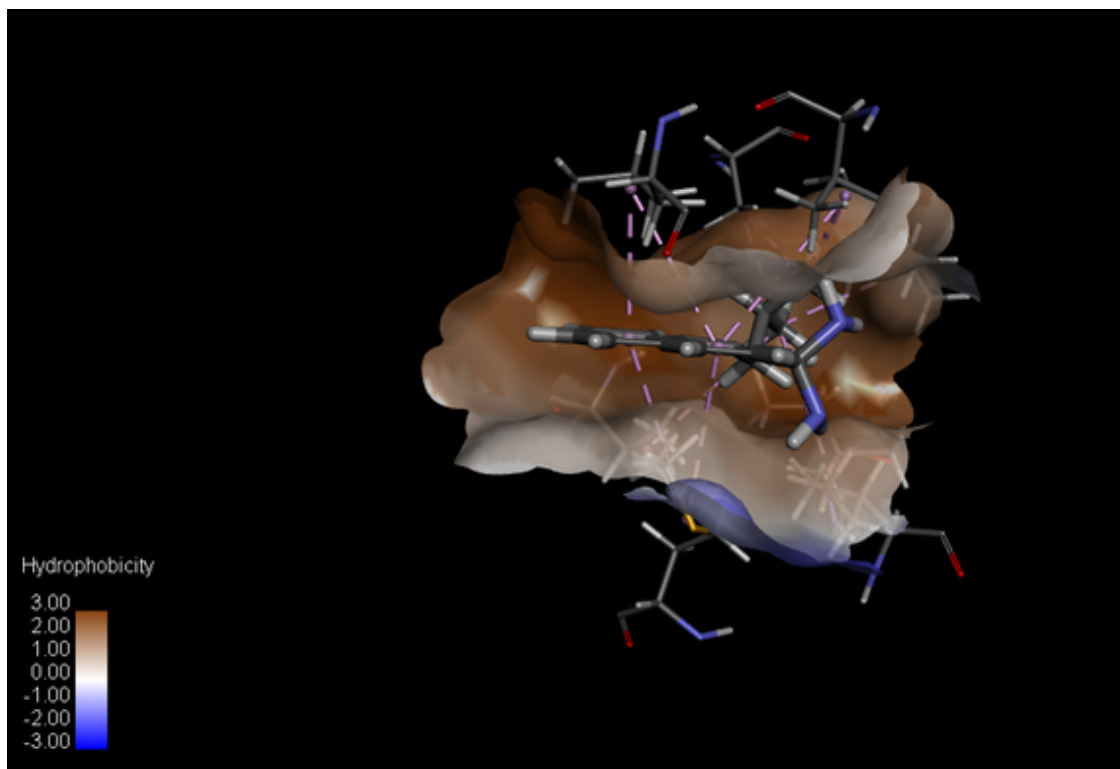


Figure 17: Hydrophobicity levels of the receptor-ligand interactions between DAPK1 and the *de novo*-generated ligand. Areas of high hydrophobicity are depicted in shades of brown, with white being areas of neutral hydrophobicity, and shades of blue being areas of low hydrophobicity.

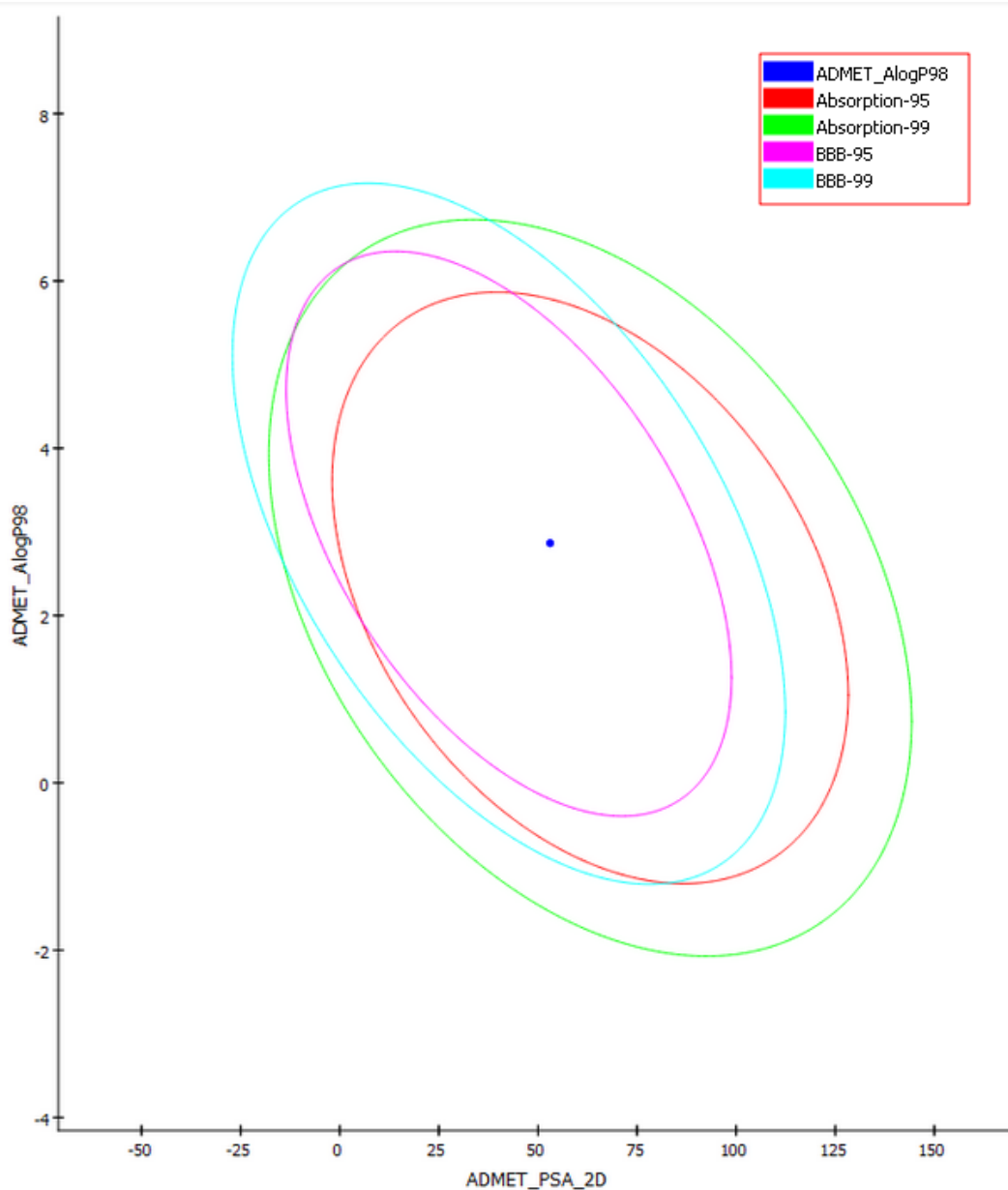


Figure 18: ADMET plot for the *de novo*-generated ligand. The key at the top right indicates what each color refers to. The blue dot is the ADMET score of the pharmacophore-generated ligand as compared to the molecular properties calculated. The red and green circles refer to its absorption abilities. The purple and light blue circles refer to the permeability through the blood brain barrier..

5 Critical Analysis

It is important when analyzing the two ligands generated to compare them to known inhibitors and other ligands.

After producing the two optimal ligands using both the pharmacophore-based strategy and the *de novo*-based strategy, they were compared through hydrophobicity levels, their receptor-ligand interactions with the 1WVX structure, their binding energy to the ATP-binding pocket, and their ADME properties. They were also compared with a negative control (thrombin inhibitor), positive controls (kinase ligands), and other inhibitors (OSV and the original inhibitor in the 1WVX structure).

5.1 Analyzing Control Groups

The first control looked at was DAPK1 and a kinase ligand. This kinase ligand is non-selective. This control acts as both a positive and negative control. This ligand should bind to the kinase domain, but because it is non-selective, it shouldn't be used as a positive control in terms of selectivity. Figure 19 shows the receptor-ligand interactions between this kinase ligand and DAPK1. There are a lot less intermolecular interactions and most of them are not pi-interactions. This shows that the kinase ligand will still bind but probably for not as long as the generated ligands. The generated ligands have many more interactions and on average, they are much stronger than the interactions seen in Figure 19. The binding energy for this complex is -74.6 kcal/mol, suggesting that binding is not unfavourable.

The second control looked at was between DAPK1 and a thrombin inhibitor. This is the only negative control. Thrombin is a blood-coagulation factor and not related to kinases. Thus, the inhibitor should not act very favorably towards this kinase. As can be seen in Figure 20, very few interactions are made. The binding energy is also -424.6 kcal/mol which is very low, indicating unfavorable binding. It also is a very large molecule, increasing the chances of steric clash and conformational tension since it is not designed to fit inside a kinase.

Figure 21 is looking at an octahedral ruthenium(II) ligand. This ligand contains a stable metal. It is known to interact not exactly at the ATP binding region, but close enough to the glycine-rich region to confer high selectivity and placed enough inside the receptor that it does not react with the solvent and lose its potency. The entire inhibitor is called ruthenium octasporine ligand (OSV)[4]. This drug has not been used therapeutically. This drug is a positive control because it exhibits high potency and selectivity. The binding energy of this complex is -50 kcal/mol, suggesting favorable binding. Although it binds to a small number of residues, it makes many interactions, suggesting very strong binding and decreased probability of steric clash.

The next thing to understand was whether or not the generated ligands exhibit some kind of selectivity. The approach used to test this was docking the pharmacophore-generated and *de novo*-generated ligands to a different kinase, such as protein kinase C [8]. Figure 22 shows an image of the receptor-ligand interaction between the pharmacophore-generated ligand and PKC. The binding energy is -78.7 kcal/mol, which is very similar to the binding energy of the pharmacophore-generated ligand and DAPK1. This suggests that energetically, the ligand is just as likely to bind to PKC as DAPK1. This is not a desired consequence

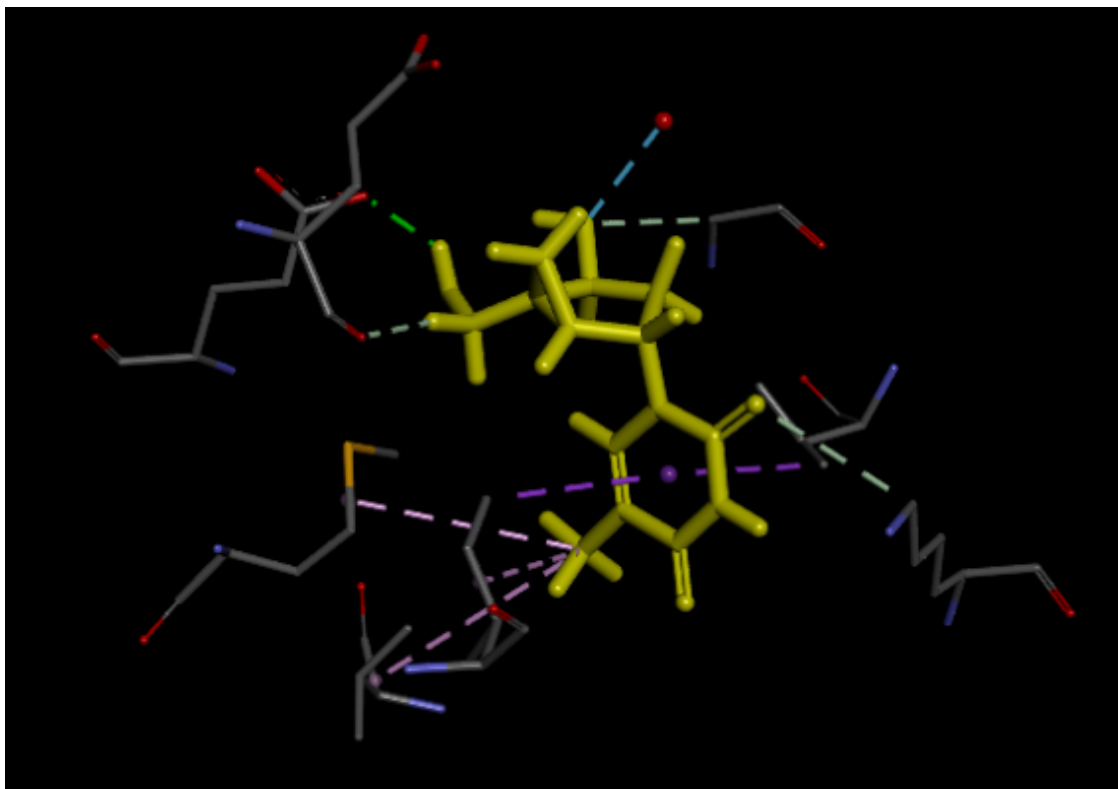


Figure 19: Receptor-ligand interaction between a non-selective kinase ligand and DAPK1. Purple dashed lines represent pi-interactions. Green dashed lines represent hydrogen bonds between non-water molecules. Blue dashed lines represents hydrogen bonds between water molecules and non-water molecules. White dashed lines represents charged interactions.

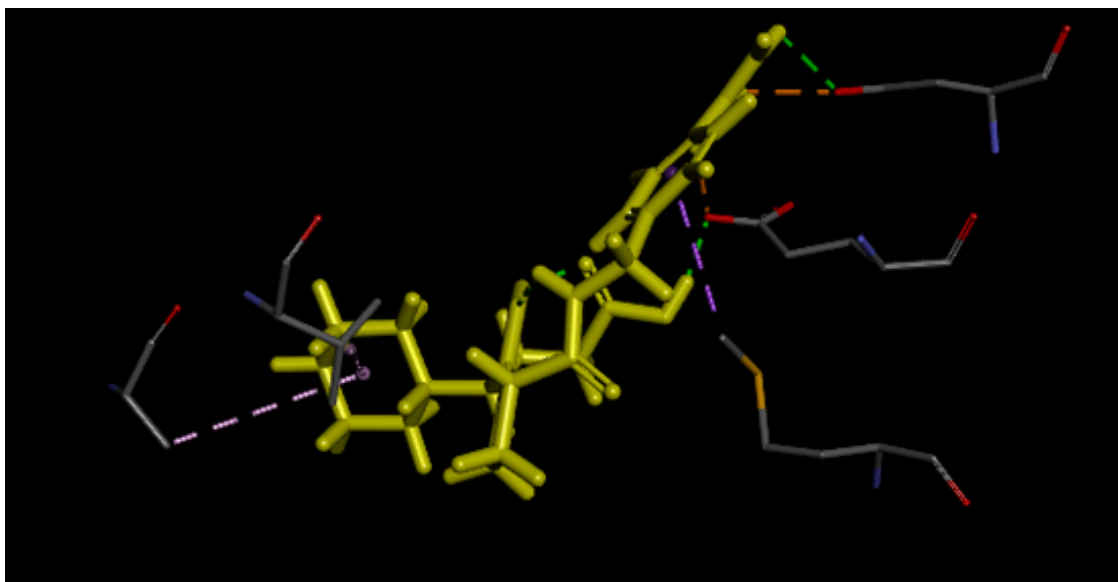


Figure 20: Receptor-ligand interactions between DAPK1 and a thrombin inhibitor. Purple dashed lines represent pi-interactions. Green dashed lines represent hydrogen bonds between non-water molecular interactions. Orange dashed lines represent charged interactions. The inhibitor in this image does not look like it is in an energetically favorable conformation.

but is still speculative. Further wetlab studies will have to prove this. The receptor-ligand interactions show a strong amount of intermolecular interactions.

Figure 23 shows the receptor-ligand interactions of the *de novo*-generated ligand and PKC. The binding energy of this complex is -39.9 kcal/mol which suggests less favorable binding than the pharmacophore-generated ligand to PKC. Figure 23 also demonstrates very few intermolecular interactions between the *de novo*-generated ligand and PKC. This suggests that this ligand is less selective to PKC and would not have a strong potency for PKC inhibition.

5.2 Choosing the Best Ligand

Based on the receptor-ligand interactions, the hydrophobicity, the structure of the ligand, the binding energies, the ADMET plots, and the comparisons between control groups, we believe that the best ligand generated is the *de novo*-generated ligand.

The *de novo*-generated ligand makes many intermolecular interactions with DAPK1 (Figure 16). Given the size of the pharmacophore-generated ligand, it is expected that it would make more contacts to DAPK1 (Figure 12). However, most of the interactions occur because of the aromatic rings and only a few interactions stem from the tail of the pharmacophore-ligand. The *de novo*-generated ligand makes strong pi-interactions with DAPK1, while also keeping a relatively small size, decreasing the chance of steric clash and facilitating binding and absorption into cells.

The hydrophobicity levels of both of the ligands seem fairly consistent and do not provide a good basis to choose an optimal ligand. Both have areas of high, neutral, and low

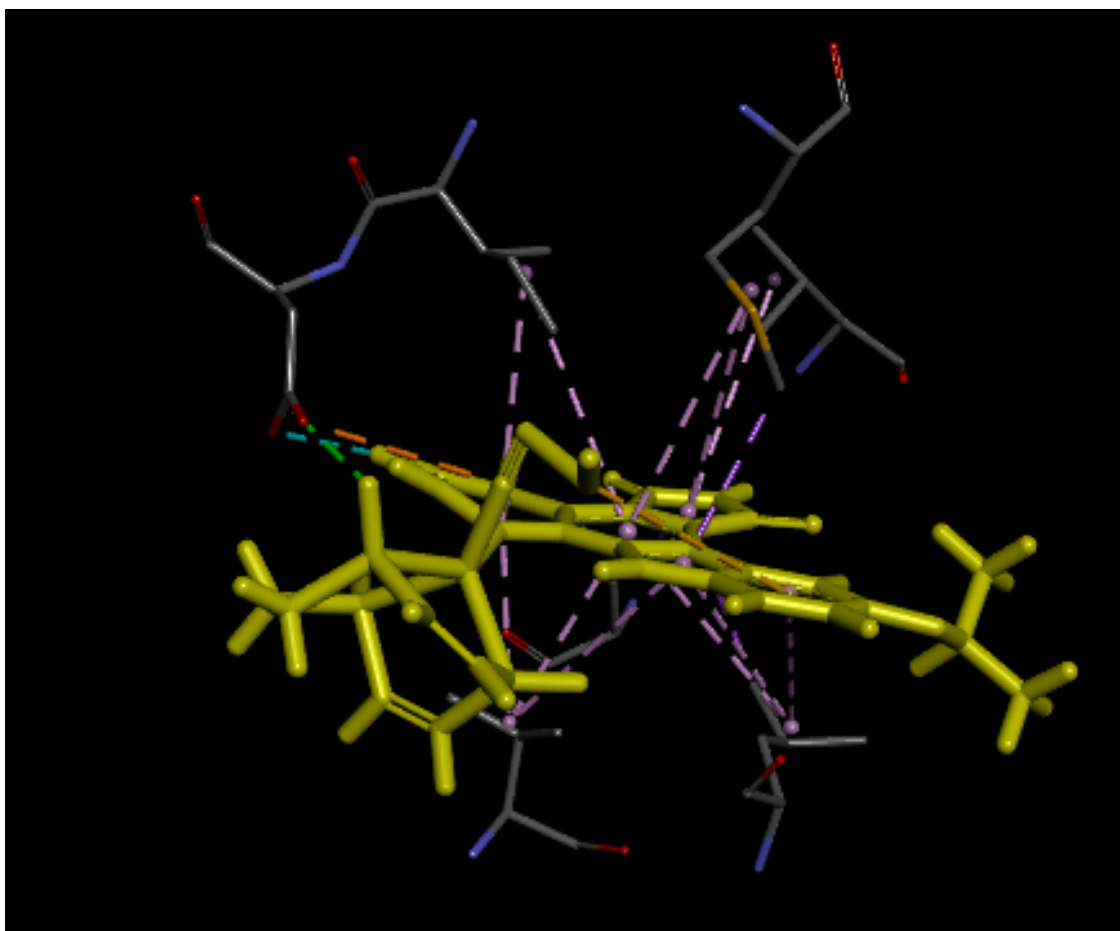


Figure 21: Receptor-ligand interaction between OSV and DAPK1. The purple dashed lines represent pi-interactions. Green dashed lines represent hydrogen bonds between non-water molecules. Orange dashed lines represent charged interactions.

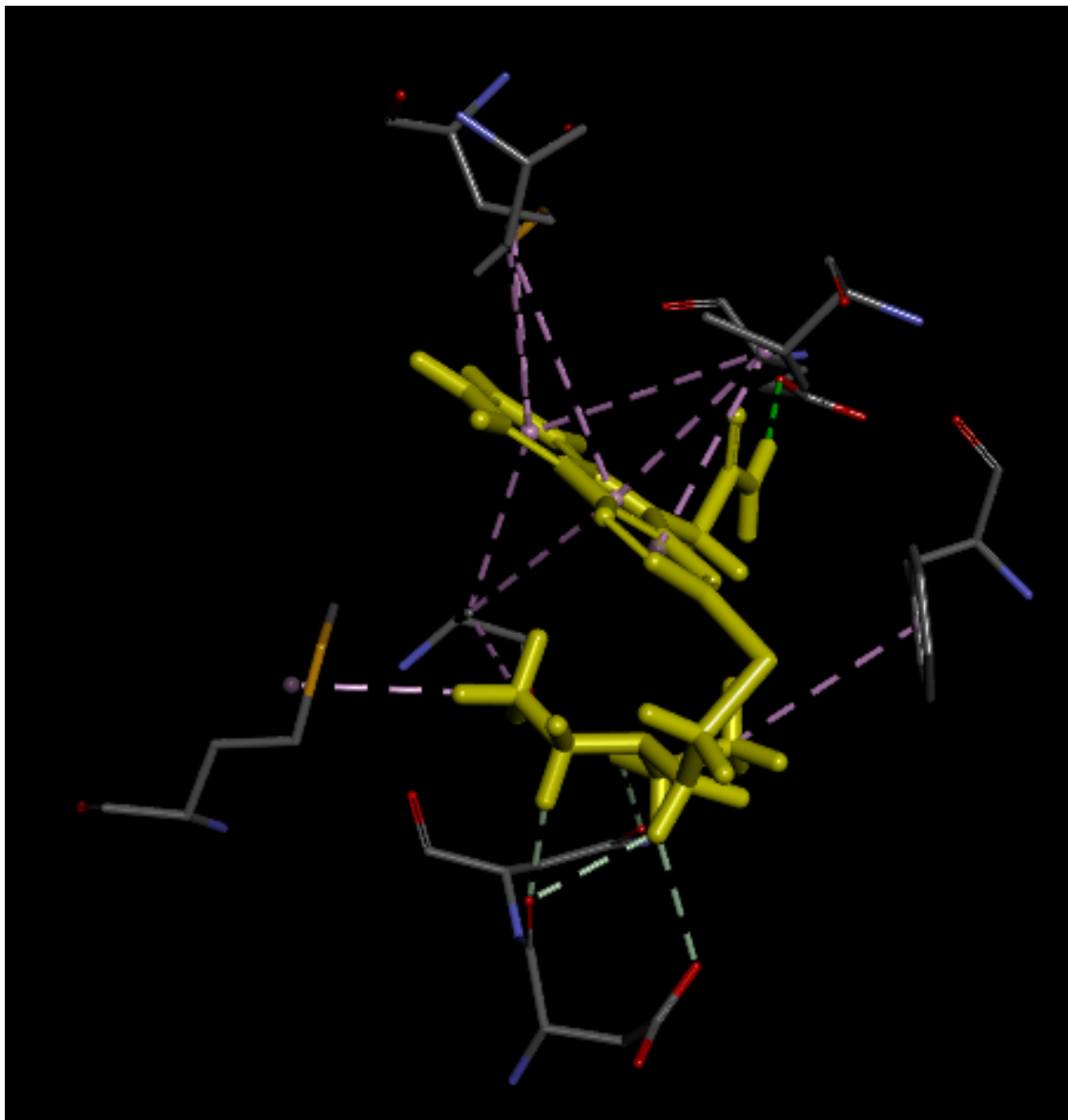


Figure 22: Receptor-ligand interaction between pharmacophore-generated ligand and PKC. Purple dashed lines represent pi-interactions. White dashed lines represent conventional bonds.

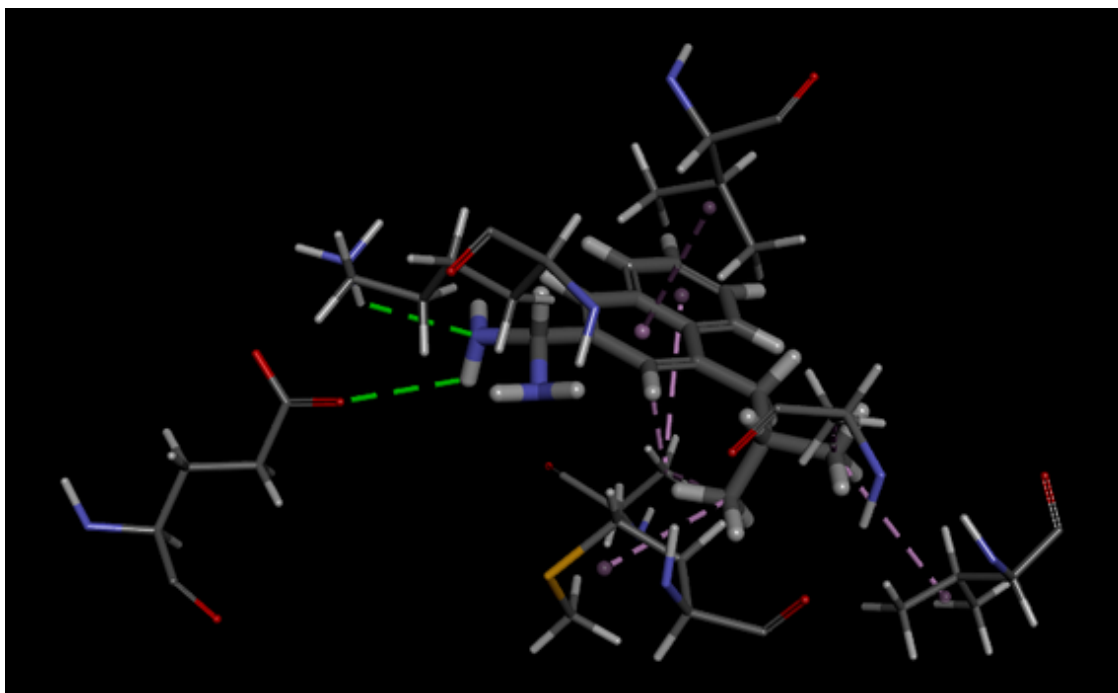


Figure 23: Receptor-ligand interaction between *de novo*-generated ligand and PKC. Green dashed lines represent hydrogen bonds between non-water molecules. Purple dashed lines represent pi-interactions.

hydrophobicity. It does not seem like one is more hydrophobic than the other.

The structure of the ligand helped determine which ligand is optimal. The pharmacophore-generated ligand is much bigger and more complex than the *de novo*-generated ligand, suggesting that it may be more difficult to synthesize. It contains a sulfur atom, six nitrogen atoms, one oxygen atom, and three aromatic rings with many double bonds and non-carbon atoms. The middle pentene ring also contains a complex functional group involving a carbonyl and an amine. The *de novo*-generated ligand contains two aromatic rings and two nitrogen atoms. The side chain of the *de novo*-generated ligand can be easily added to the functionalized naphthalene. Compared to the pharmacophore-generated ligand, the *de novo*-generated ligand is much easier to synthesize.

Based on the binding energies, the pharmacophore-generated ligand (-78.9 kcal/mol) exhibits more favourable binding than the *de novo*-generated ligand (-7 kcal/mol). This was the only source of conflict between choosing the *de novo*-generated ligand as the optimal ligand because its binding energy is so low. This could present a problem when determining the potency of the *de novo*-generated ligand and whether or not a higher concentration would need to be administered. Ideally, the smaller the concentration given to the patient, the better as it may cause less non-selectivity and less side effects.

The ADMET plots of the ligands (Figures 14 and 18) suggest that the *de novo*-generated ligand fits the data much better than the pharmacophore-generated ligand. Because it fits the data better, it may also have a higher tolerance to be taken orally which is a much better standard than injecting drugs. By having an orally bioavailable drug, the patient standard

of care is increased dramatically. The pharmacophore-generated ligand may also be orally bioavailable but it lies very close to the BBB-95 circle (Figure 14).

The biggest indicator that the *de novo*-generated ligand outcompetes the pharmacophore-generated ligand is that it is more selective to DAPK1 than PKC. The binding energy between DAPK1 and the *de novo*-generated ligand is substantially smaller than the pharmacophore-generated ligand to PKC. The *de novo*-generated ligand also makes less intermolecular interactions to PKC than the pharmacophore-generated ligand decreasing its potency against PKC inhibition and affinity for it.

6 Conclusion

The biggest difference between the pharmacophore-generated ligand and the *de novo*-generated ligand protocol was that the former was much more automated than the latter. During the *de novo*-generated ligand protocol, there were many more opportunities to edit the ligand. Editing the ligand manually seemed to increase the selectivity of the drug to the ATP binding site and ultimately created a stronger ligand. Given enough time, other functional groups or aromatic rings could have been added to the *de novo*-generated ligand based on surrounding residues.

Many ligands and their conformations were eliminated solely based on their Libdock or CDOCKER score; because of this, some ligands may have been eliminated that would have fit better in the ATP binding site. Given enough time, all of the ligands outputted by the chemdiv screen would be used in ligand docking algorithms. It may have also been more optimal to create the pharmacophore manually, while placing emphasis on the residues around the ATP binding site.

Another strategy that may have benefited this experiment would have been searching for other binding sites that could have inhibited function. The only binding sites looked at were ATP binding sites, but there are many other domains important for catalysis. For example, a ligand may inhibit a structural rearrangement rather than a chemical reaction. By studying global and local movements of residues, a ligand could have been created to impede a movement, thus inhibiting kinase function. However, it is computationally difficult to study the mechanisms of inhibition that would have occurred when the ligands bound because x-ray crystallography does not output data on the kinetics of protein mechanisms.

This experiment taught me much about *in silico* chemistry. It is an excellent step to perform before wetlab research. Looking at specific residues and rationally designing a ligand catered to a specific active site would decrease the amount of time to create a drug and continue onto clinical trials. It also utilizes algorithms and databases to generate ligands at a much faster rate than human capacity would allow.

Another novel design approach I learned was generating pharmacophores. It seems that it allowed for more opportunity to create a ligand based on the properties I want it to exhibit. These properties could be based on surrounding residues and interactions. Instead of designating a particular atom, I could create a pharmacophore with certain chemical properties and then use this as a blueprint to generate a ligand library that fulfills these requirements. Because a pharmacophore only requires chemical properties at certain locations, the diversity of the pharmacophore-generated ligand library is much more diverse than a *de novo*-generated

ligand library.

I also learned how important it is to minimize the energy of a molecule and place it in its most energetically stable conformation. It was also interesting to see that all of the ligand docking algorithms utilized many different conformations of the same ligand to optimize the interaction. I did not think slightly different conformations would drastically change the interaction between the kinase and the inhibitor.

References

- [1] Bialik, S. & Kimchi, A. The death-associated protein kinases: structure, function, and beyond. *Annu. Rev. Biochem.* 75, 189–210 (2006).
- [2] Bialik, S. & Kimchi, A. DAP-kinase as a target for drug design in cancer and diseases associated with accelerated cell death. *Semin. Cancer Biol.* 14, 283–294 (2004).
- [3] Tereshko, V., Teplova, M., Brunzelle, J., Watterson, D. M. & Egli, M. Crystal structures of the catalytic domain of human protein kinase associated with apoptosis and tumor suppression. *Nat. Struct. Biol.* 8, 899–907 (2001).
- [4] Feng, L. et al. Structurally sophisticated octahedral metal complexes as highly selective protein kinase inhibitors. *J. Am. Chem. Soc.* 133, 5976–5986 (2011).
- [5] McNamara, L. K., Brunzelle, J. S., Schavocky, J. P., Watterson, D. M. & Grum-Tokars, V. Site-directed mutagenesis of the glycine-rich loop of death associated protein kinase (DAPK) identifies it as a key structure for catalytic activity. *Biochimica et Biophysica Acta (BBA) - Molecular Cell Research* 1813, 1068–1073 (2011).
- [6] PDB ID: 1WVX. Ueda, Y., Ogata, H., Yamakawa, A., Higuchi, Y. <http://pdb.org/pdb/explore/explore.do?structureId=1wvx>.
- [7] Balani, S. K., Miwa, G. T., Gan, L.-S., Wu, J.-T. & Lee, F. W. Strategy of utilizing in vitro and in vivo ADME tools for lead optimization and drug candidate selection. *Curr Top Med Chem* 5, 1033–1038 (2005).
- [8] Grodsky, N. et al. Structure of the catalytic domain of human protein kinase C beta II complexed with a bisindolylmaleimide inhibitor. *Biochemistry* 45, 13970–13981 (2006).